

Supporting Information

High-Rate Capability of Na₂FePO₄F Nanoparticles by Enhancing Surface Carbon Functionality for Na-Ion Batteries †

Jesse S. Ko,^{a,e} Vicky V. T. Doan-Nguyen,^{b,c} Hyung-Seok Kim,^a Xavier Petriessans,^a Ryan H. DeBlock,^a Christopher S. Choi,^a Jeffrey W. Long,^d and Bruce S. Dunn^{*a}

^a Department of Materials Science and Engineering, University of California, Los Angeles, Los Angeles, CA 90095, United States

^b California NanoSystems Institute, University of California, Santa Barbara, Santa Barbara, Santa Barbara, CA 93106, United States

^c Materials Research Laboratory, University of California, Santa Barbara, Santa Barbara, Santa Barbara, CA 93106, United States

^d U.S. Naval Research Laboratory, Surface Chemistry Branch (Code 6170), Washington, DC, 20375, United States

^e U.S. Naval Research Laboratory–National Research Council Postdoctoral Associate, Washington, DC, 20375, United States

***Corresponding author:** Bruce S. Dunn

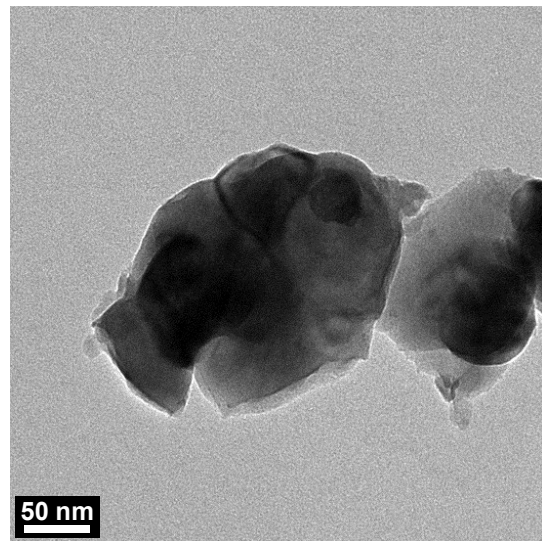


Fig. S1. Transmission electron micrograph of NFPP-SSR.

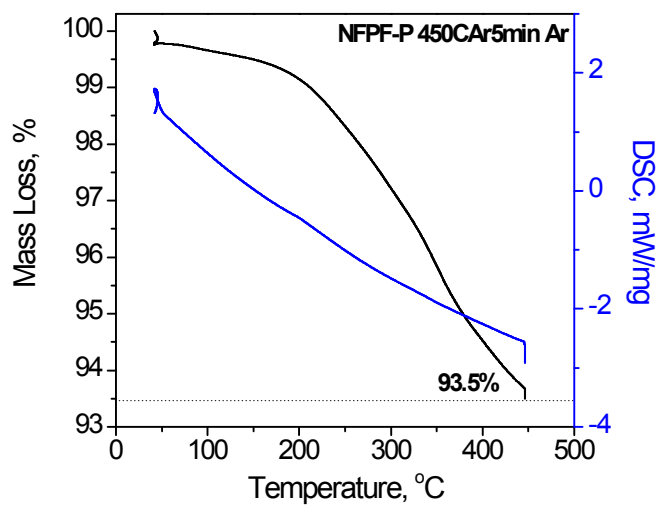


Fig. S2. Thermogravimetric analysis/differential scanning calorimetry of NFPP-P heat-treated at 450 °C under an inert atmosphere (argon) with an isothermal hold for 5 min at 450 °C.

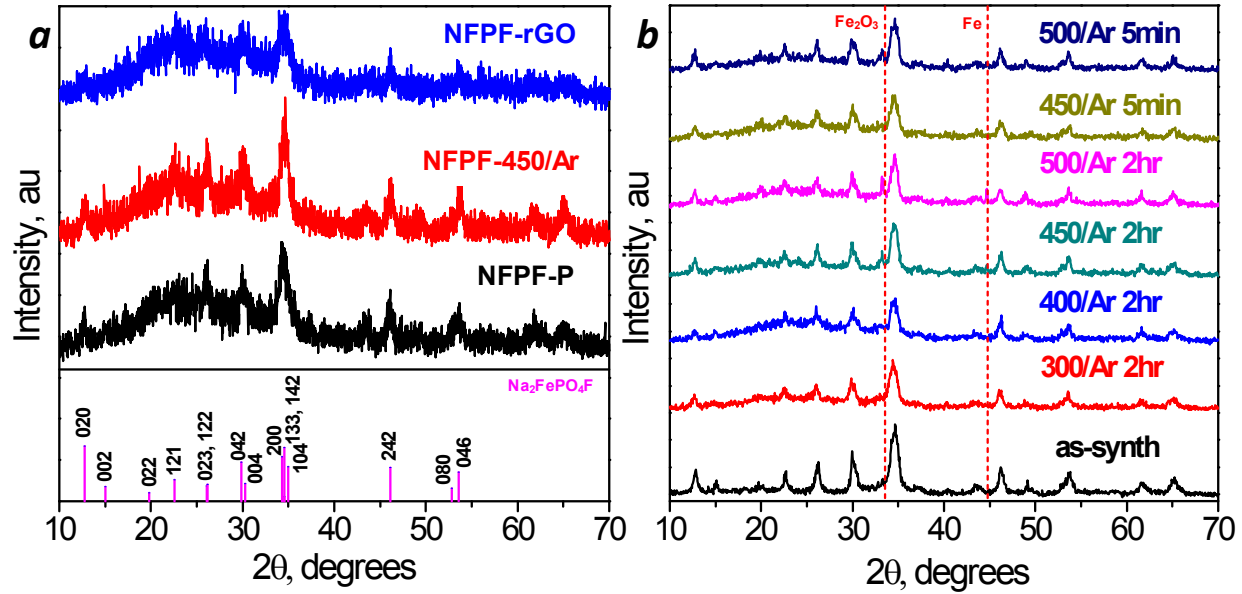


Fig. S3. **(a)** The X-ray diffraction phase analysis of the polyol-derived NPPF-P, argon-treated NPPF-450/Ar, and NPPF-rGO nanocomposite. **(b)** The X-ray diffraction patterns of NPPF-P heat-treated at various temperatures. Dotted red line indicates early stages of decomposition leading to oxidized Fe_2O_3 and metallic Fe.

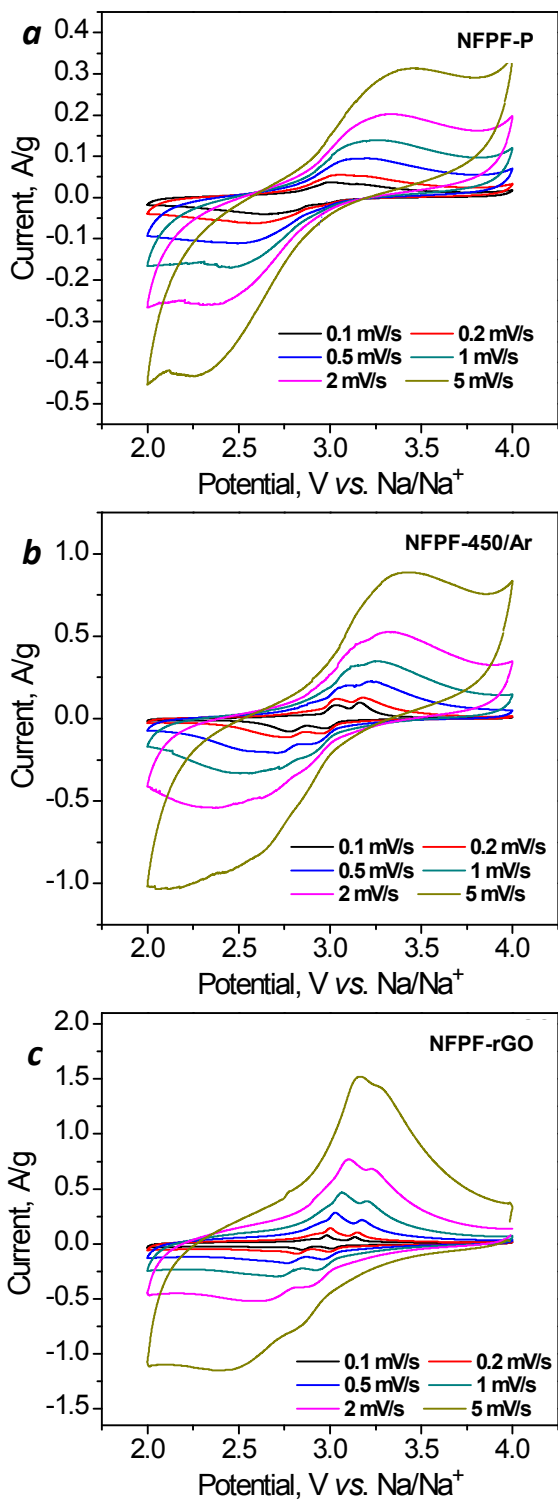


Fig. S4. Cyclic voltammograms of (a) NPFF-P, (b) NFPP-450/Ar, and (c) NFPP-rGO cycled between 2.0–4.0 V vs. Na/Na⁺ from 0.1–5 mV s⁻¹.

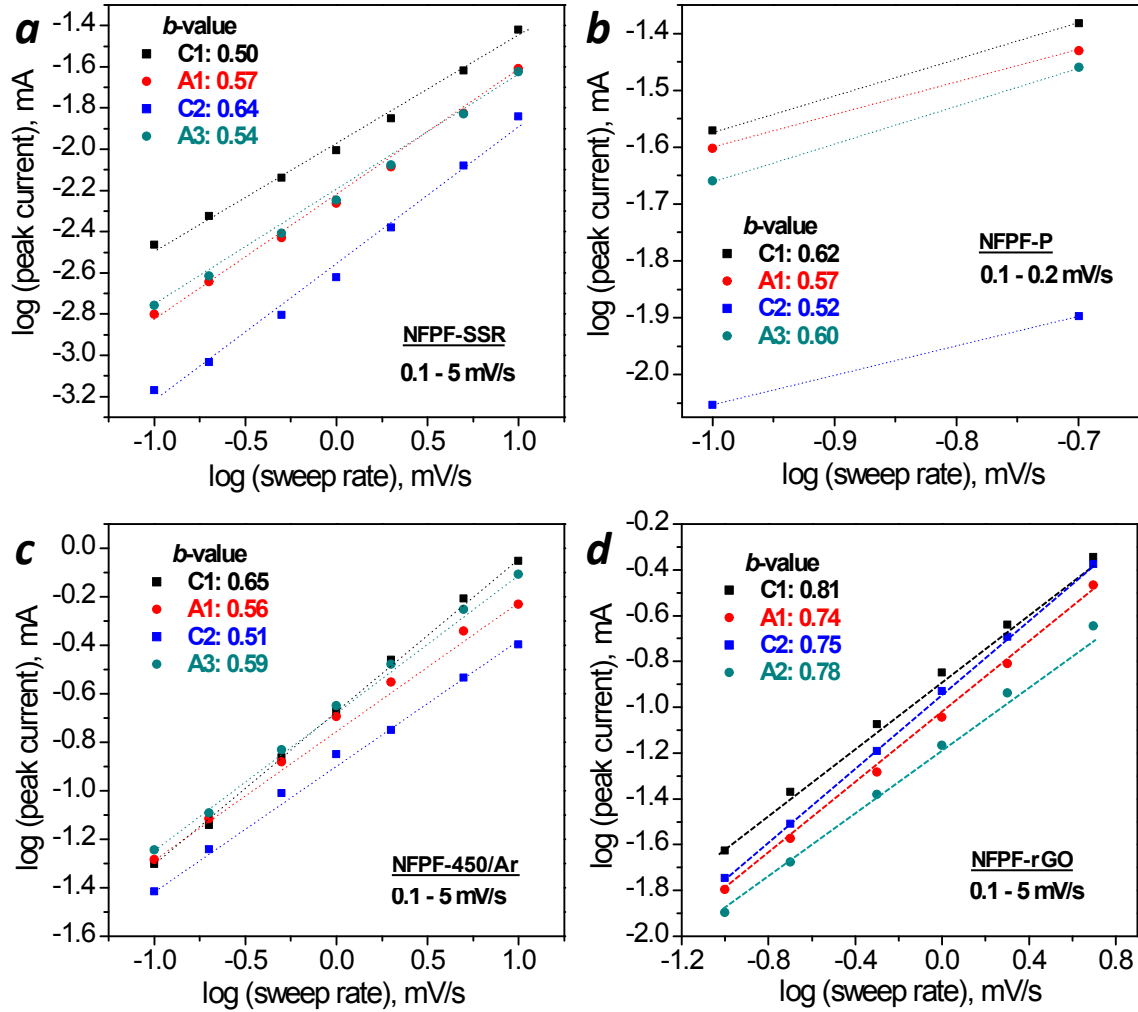


Fig. S5. The b -value analysis [$\log(i)$ vs. $\log(v)$] of (a) NFPF-SSR, (b) NFPF-P, (c) NFPF-450/Ar, and (d) NFPF-rGO.

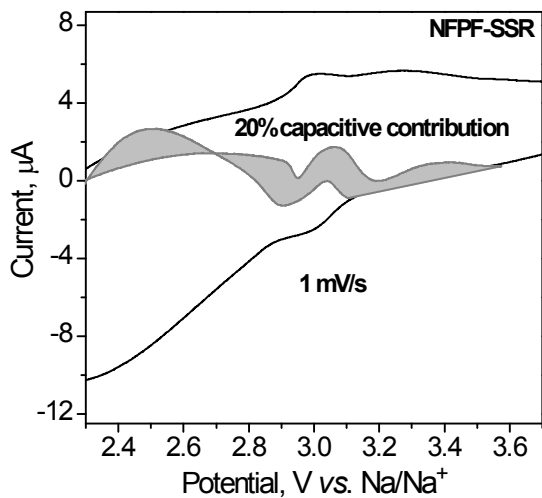


Fig. S6. Capacitive contribution determination of NPPF-SSR cycled at 1 mV s^{-1} .

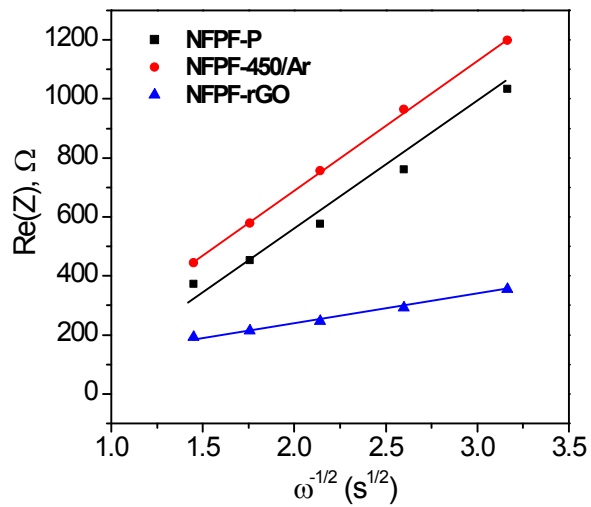


Fig. S7. Determining the Warburg coefficient by the slope of the line in a plot of $\text{Re}(Z)$ vs. $\omega^{-1/2}$.

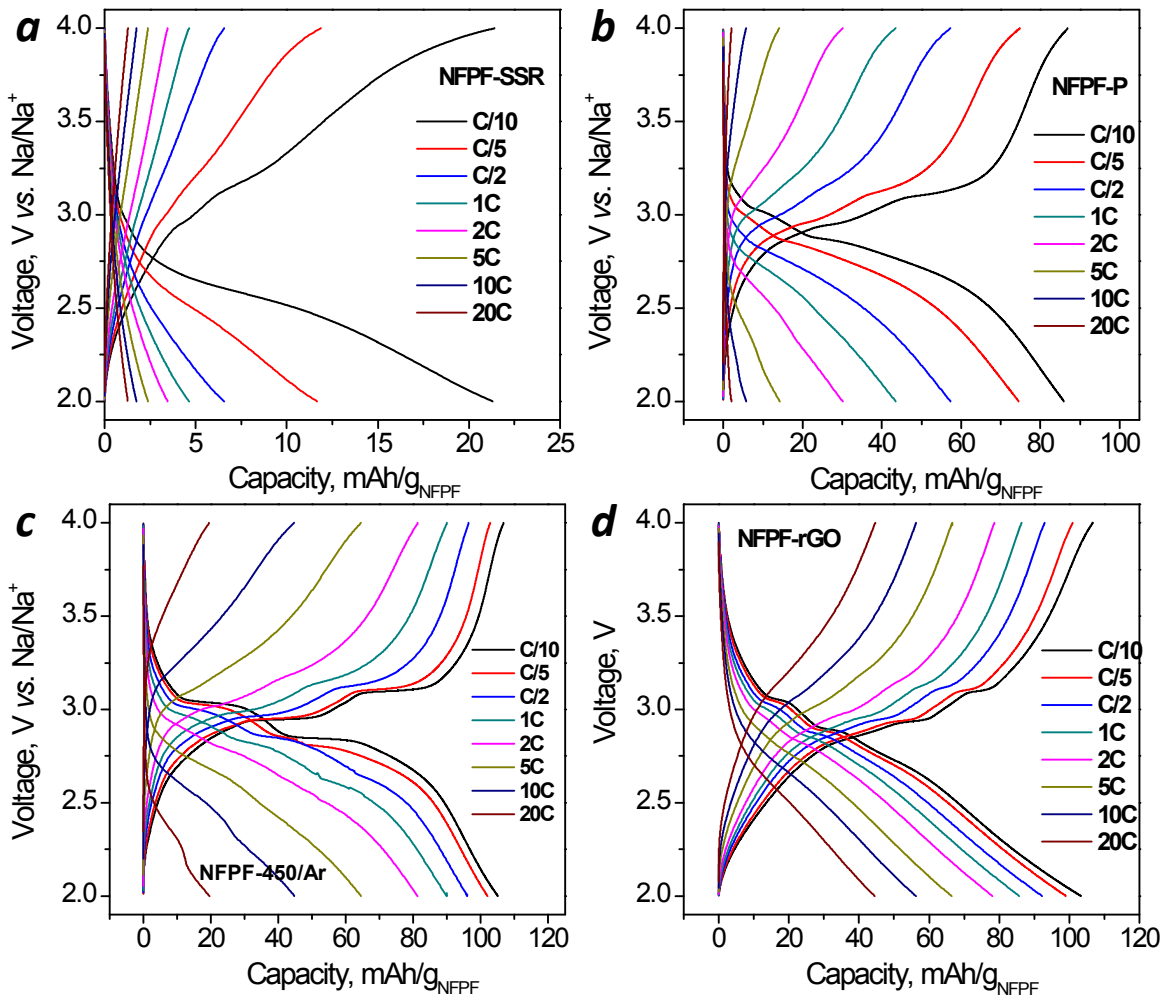


Fig. S8. Galvanostatic charge–discharge curves of (a) NFPF-SSR, (b) NFPF-P, (c) NFPF-450/Ar, and (d) NFPF-rGO with C-rates imposed from C/10 to 20C.

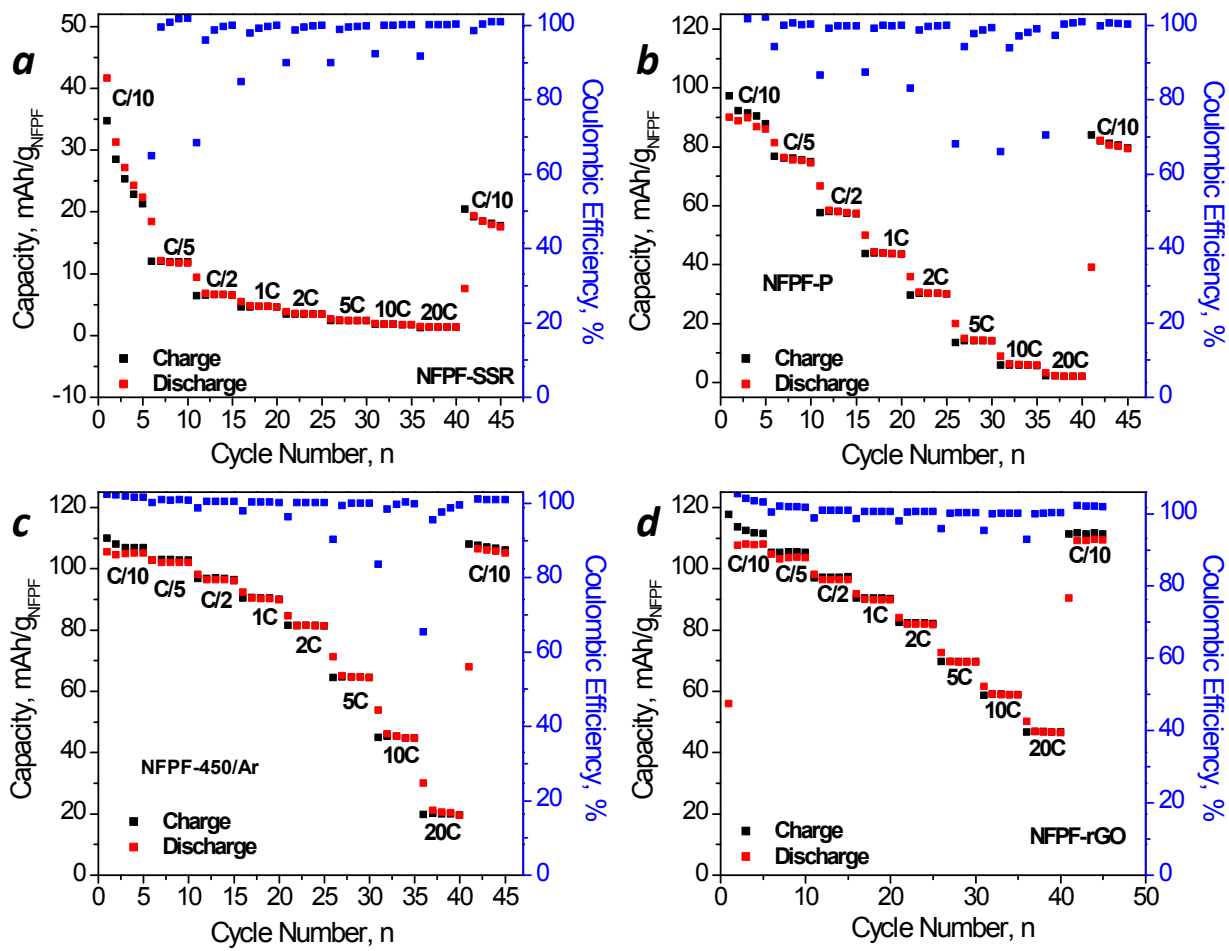


Fig. S9. Galvanostatic cycling performance of (a) NFPF-SSR, (b) NFPF-P, (c) NFPF-450/Ar, and (d) NFPF-rGO measuring specific capacities and coulombic efficiencies from C/10 to 20C.